CrystEngComm

Accepted Manuscript

ROYAL SOCIETY OF CHEMISTRY

www.rsc.org/crystengcomm

CrystEngComm

ARTICLE

New Ni(II) 1,2-bis(diphenylphosphino)ethane dithiolates: Crystallographic, computational and Hirshfeld surface analyses

Received 00th January 20xx,
Accepted 00th January 20xx

DOI: 10.1039/x0xx00000x

www.rsc.org/

Reena Yadav,[a] Manoj Trivedi,[b] Gabriele Kociok-Köhn,[c] Rajendra Prasad[d] and Abhinav Kumar[a]*

Three new nickel(II) 1,2-bis(diphenylphosphino)ethane dithiolate complexes *viz*. [Ni(dppe)(benzylcyanidedithiolate)] (**1**), [Ni(dppe)(2-cyanobenzylcyanidedithiolate)] (**2**) and [Ni(dppe)(pyridine-2-cyanidedithiolate)] (**3**) have been synthesized and characterized spectroscopically and by single crystal X-ray. The X-ray analyses for **2** and **3** reveal a distorted square planar geometry around Ni(II) satisfied by the two sulfur atoms of the dithiolate and two phosphorus atoms of the dppe ligands. Both **2** and **3** display intermolecular C-N···H, π···π and C-H···π and C-S···H interactions which generates a supramolecular framework. Additionally, both **2** and **3** shows intramolecular C-H···Ni anagostic interactions. These interactions have been addressed by *ab initio*, AIM, Hirshfeld surface analyses. The anagostic interaction was verified using bond order and natural charge calculations which indicated depletion of electron density on the *ortho*-hydrogen atoms undergoing the anagostic interactions. All three compounds exhibit photoluminescence in dichloromethane solution as well as in solid state. The solid state emissions are red shifted in comparison to the solution phase emissions which may be attributed to the existence of inter-molecular interactions in solid state.

Introduction

Metal dithio complexes are very attractive compounds for the synthetic and crystal engineers[1] due to their structural diversity.[2] They show good conducting,[3] magnetic,[4] and optical properties[5] and serve well as a single source precursors for the preparation of metal sulphides[6] as photocatalysts in solar energy schemes,[7] and for organic synthesis.[8] The recent growing interest in dithiolate chemistry is down to the functionalization of the dithio backbone that may generate fascinating supramolecular architectures in the crystalline state which are capable of displaying modified physical properties.[1-8] Crystal engineering of the metal directed self-assembly of coordination compounds afforded by S···H, O···H, N···H, S···S, π···π and C–H···π (chelate, CS_2M) secondary interactions play a key role in the organization of supramolecular networks. [9-11]

Amongst 1,1-dithiolates, a great deal of attention has been paid to the monoanionic xanthate, dithiocarbamate and dithiophosphate and dianionic 1,1-ethylenedithiolate type ($XYC{=}CS_2^{2-}$).[1-8] Recently, multimetallic assemblies have been prepared using a piperazine-based dithiocarbamate building block and Ni(dppe)Cl_2 by Wilton-Ely and Hogarth *et al.*.[12] These system have been utilized for the functionalization of gold nanoparticles.[13] Inspired by these investigations we recently found the 1,2-*bis*(diphenylphosphino)ethane nickel(II) dithiocarbamates be a potential precursor for nickel sulphide and also investigated the effect of counter anions on the phase and morphology of the synthesized nickel sulfides.[14] Despite the synthetic versatility and practical utility metal complexes of dianionic 1,1-dithiolates derived from active methylene group attached to the cyano and phenyl group are relatively rare and only a few structural characterization and photoluminescent properties of a Pt(II) complex with Di-*tert*-butyl bipyridine have been reported.[15] Therefore, we considered it to be worthwhile to synthesise, determine the crystal structures and study the photoluminescence behaviour of the heteroleptic Ni(II) complexes formed with three different dianionic dithiolates and 1,2 *bis*(diphenylphosphino)ethane (dppe) which have been used as co-ligands. These newly synthesized 1,1-ethylene dithiolate type ligands with substituted phenyl/pyridyl rings enhance conjugation with different extent of delocalization of negative charge over the aromatic ring and can provide greater electron delocalisation through the C-S, C-C and beyond the MS_2 bond. Thus, the functionalization of the aromatic ring may induce new intra- and intermolecular non-covalent interactions, thereby generating new supramolecular architectures and possibly may lead to different optoelectronic properties. Metal complexes containing *tertiary*-phosphine ligands have played an important role in catalytic reactions.[16] Furthermore, the steric and electronic properties of dithiolates in conjunction with dppe ligands may noticeably influence their structural features and properties. The interesting C≡N···H, C-S···H, π···π and C-H···π intermolecular interactions and rare

[a] Department of Chemistry, University of Lucknow, Lucknow 226 007, India.
[b] Department of Chemistry, University of Delhi, Delhi 110 007, India.
[c] Department of Chemistry, University of Bath, Bath BA2 7AY, UK.
[d] Department of Chemistry, S. G. B. University, Amrawati, Maharashtra, India.
† Footnotes relating to the title and/or authors should appear here.
Electronic Supplementary Information (ESI) available: [details of any supplementary information available should be included here]. See DOI: 10.1039/x0xx00000x

intramolecular C-H···Ni anagostic interaction have been described herein.[11] Attempts have been made to address the nature of these interactions using quantum chemical calculations and Hirshfeld surface analysis.[17]

Results and discussion

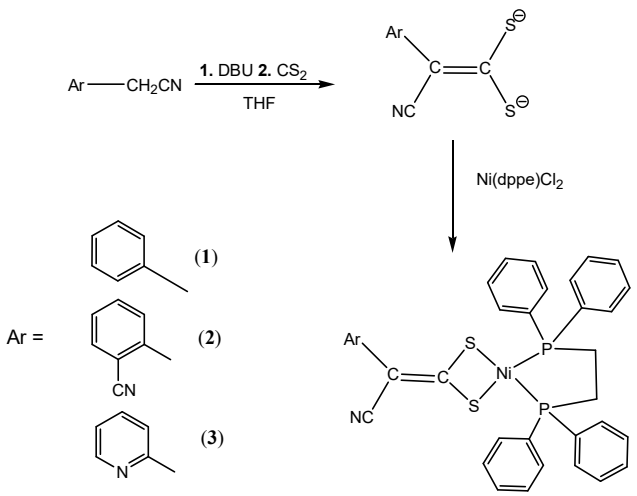

Scheme 1. Synthetic routes for the preparation of the complexes.

Synthesis

The three dianionic dithiolate ligands were prepared *in situ* by addition of 1,8-Diazabicyclo[5.4.0]undec-7-ene (DBU) followed by addition of carbon disulfide to the corresponding aromatic acetonitriles *viz.* phenylacetonitrile, 2-cyano methyl benzonitrile and pyridine-2-acetonitrile dissolved in THF under nitrogen atmosphere. The resulting solution was added dropwise to the dichloromethane solution of Ni(dppe)Cl_2 to obtain the corresponding Ni(II) 1,2-bis(diphenylphosphino)-ethane dithiolates (Scheme 1). All three compounds were air stable and soluble in halogenated solvents but insoluble in alcohols and ether.

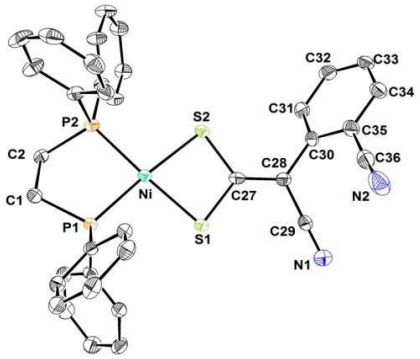

Fig. 1 ORTEP view of the molecular structure of 2. Atoms are drawn at 30% probability. Solvent molecule and hydrogen atoms are removed for clarity.

Spectroscopy

The IR spectra for all the three compounds display bands at ~ 2200, 1440 and ~1100 cm^{-1} which corresponds to the ν C≡N, ν C=CS_2 and νCS_2 vibrations a characteristic feature of dithiolate ligands. Existence of single vibration at ~1100 cm^{-1} indicates the bonding of dithiolate ligand to Ni(II) center in symmetrical bidentate mode. The purity and composition of all the three compounds were checked by ^{1}H NMR spectroscopy. All of the compounds display well resolved ^{1}H NMR signals which integrate to the corresponding hydrogen atoms. The signals at ~ δ 182-190 ppm are indicative of the CS_2 carbon of the dithiolate ligand. In $^{31}P\{^1H\}$ NMR the presence of only one signal at ~ δ 58.9 ppm indicates symmetrical bidentate bonding mode of the dppe ligand to the Ni(II) center.

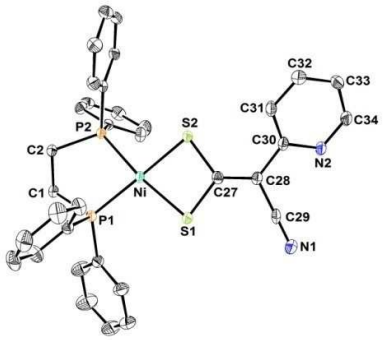

Fig. 2 ORTEP view of the molecular structure of **3** with atoms drawn at 50% probability. Solvent and hydrogen atoms are removed for clarity.

Molecular structure

Single crystals of **2** and **3** were obtained by slow evaporation of a solution of the compounds in a dichloromethane/methanol mixture (2:1). In each complex, the geometry about Ni(II) is four-coordinate with the Ni atoms bonded to two phosphorus atoms of the dppe moiety together with two sulfur atoms of the bidentate dithiolate ligand (Fig. 1 and 2). The basic structural features of both complexes are equivalent. The metal atom lies at the centre of a distorted square plane. The distortion is caused due to the small S(2)-Ni-S(1) bite angles of 79.68(4)°, and 79.58(4)° for **2** and **3**, respectively. The Ni-S lengths in the range 2.1889(11)-2.2056(11) Å for **2** and **3** indicate the symmetrical (S, S) chelating behaviour of the dithiocarbamate ligands. The Ni-P distances are in the range of 2.1500(10)-2.1688(10) Å which are within the range reported for others dithiolate complexes containing dppe.[14] The C-S bond lengths of 1.750(4) and -1.754(4) Å are considerably shorter than the C-S (1.81 Å) bond observed in the transition metal dithio complexes due to π delocalisation over the C_2S_2 unit. The chelating S_2CNi rings are tilted with an angle of 17.10° and 11.58° in complexes **2** and **3** with respect to dppe moiety.

In **2** the supramolecular structures are stabilized *via* intermolecular C≡N···H, C-S···H, π···π and C-H···π non-covalent interactions [9-11] (Fig. 3). The intermolecular C≡N···H interaction (Fig. 3a) is operating between the nitrogen atom N1 of the cyanide and hydrogen atom H20 of the aromatic ring of the dppe ligand. This interaction leads to a distance of 2.738(6) Å and an angle of ∠C29-N1···H20 156.8(4)°. In addition to

these interactions, **2** also exhibits intermolecular π···π and C-H···π interactions. The π···π interaction is operating between the aromatic rings of the dppe and the dithiolate ligands (Fig. 3a). The distance between the centroids of the two aromatic rings is 3.892 Å and that between C7···C35 is 3.263 Å. There is a C-H··· π interaction between the aliphatic hydrogen of the dppe ligand and the aromatic ring of the dithiolate ligand with a distance of 2.712 Å. Figure 3b is displaying the C-S···H and C≡N···H interactions. The S2-H13 distance is 2.924(5) Å but in this case the C≡N···H interaction is operating between the cyanide nitrogen N2 and aliphatic hydrogen H1A of the dppe ligand with a distance of 2.533(6) Å the corresponding ∠C≡N···H is 118.4(4)° which is relatively more angular than that displayed in figure 3a thereby indicating that the later interaction is probably weaker than the former.

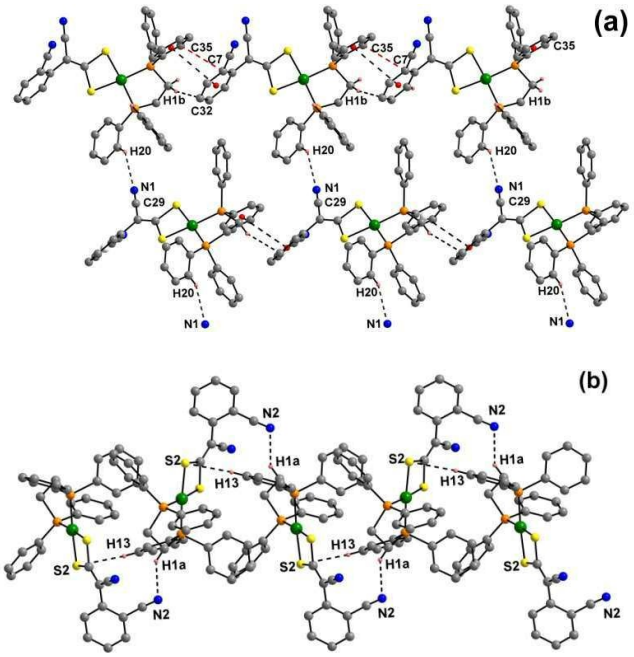

Fig. 3 Supramolecular frameworks for **2** displaying intermolecular (a) C≡N···H, π··· π and C-H··· π (b) C-S···H, C≡N···H interactions.

Like **2** the supramolecular framework in **3** is stabilized by intermolecular C≡N···H, C-S···H and C-H···π interactions[9-11] (Fig. 4). But unlike **2** it doesn't have π···π interactions. Interestingly the incorporation of the pyridine moiety in the dithiolate ligand has introduced a new (py)N···H interaction in addition to the C≡N···H bonding. The corresponding C≡N···H and (py)N···H interaction distances are 2.719(4) Å and 2.667(4) Å, respectively with an angle of ∠C29≡N1···H1B and ∠(py)C30-N2···H2B 140.3(3)° and 131.6(3)°, respectively. Unlike **2** where the C≡N···H interaction takes place between both aromatic and aliphatic hydrogens of the dppe ligand in **3** these interactions are limited to aliphatic hydrogen atoms of the dppe ligand. Like **2**, **3** is also displaying intermolecular C-S···H interactions which lead to the formation of a one dimensional chain. But no additional N···H interaction is operating as was observed in the case of **2**. The S1···H18 interactions have length 2.963 Å and ∠C27-S1···H18 is 106.96°.

Interestingly, in complexes **2** and **3**, the aromatic hydrogen atom of the dppe ligand is lying in close proximity to the metal coordination sphere forming C-H···Ni intramolecular anagostic or preagostic interactions (Fig. 5). The Ni···H-C distance and ∠Ni···H-C angles are 2.830-2.968 Å and 116.22°-119.81°, respectively which are well within the range for the anagostic interactions.[18] Unlike agostic interactions which involve 3c-2e interactions these anagostic interactions are largely electrostatic in nature (scheme 2).[18]

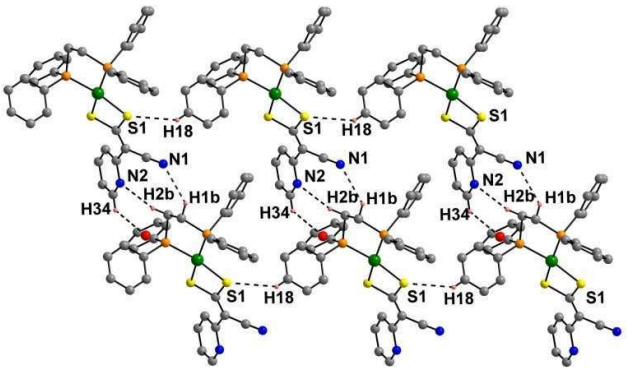

Fig. 4 Supramolecular frameworks for **3** displaying intermolecular C≡N···H; (py)N···H; C-H··· π and C-S···H interactions.

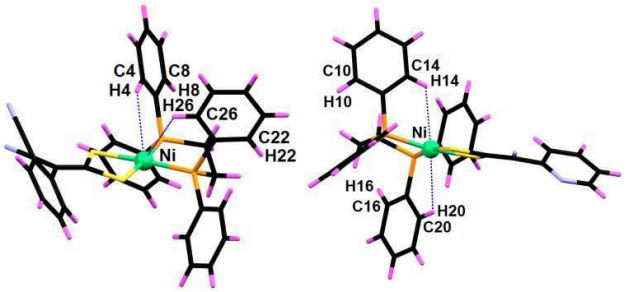

Fig. 5 Intramolecular anagostic C-H···Ni interactions for **2** (left) and **3** (right).

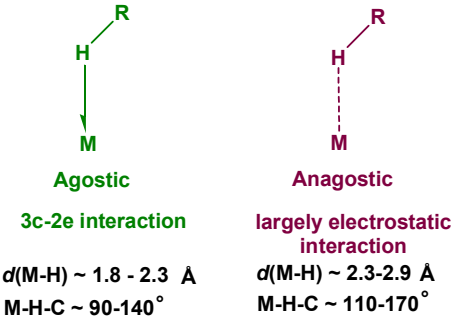

Scheme 2. Structural differences between agostic and anagostic interactions.

DFT and AIM results regarding non-covalent interactions

The crystal structures of the compounds **2** and **3** as discussed above are good examples of the interplay of different molecular interactions that lead to interesting supramolecular

aggregates in the solid state (Fig. 3 and 4). It is obvious that C≡N···H, C-S···H, π···π and C-H···π non-covalent interactions play an important role if the structure is to be rationalized in terms of interactions between the molecular fragments. However, it needs to be investigated to what kind of intermolecular interaction(s) contributes to the binding energy between molecules and dimers in the structure. It is known that the covalent, H-bond, dipole-dipole, and van der Waals interaction energies are >1700, 70 - 50, 8 - 2, and < 4 kJ/mol, respectively. In order to analyze the various interactions that lead to the crystal structure, interaction energies and electrostatic potentials have been calculated for dimers held by the aforementioned interactions.

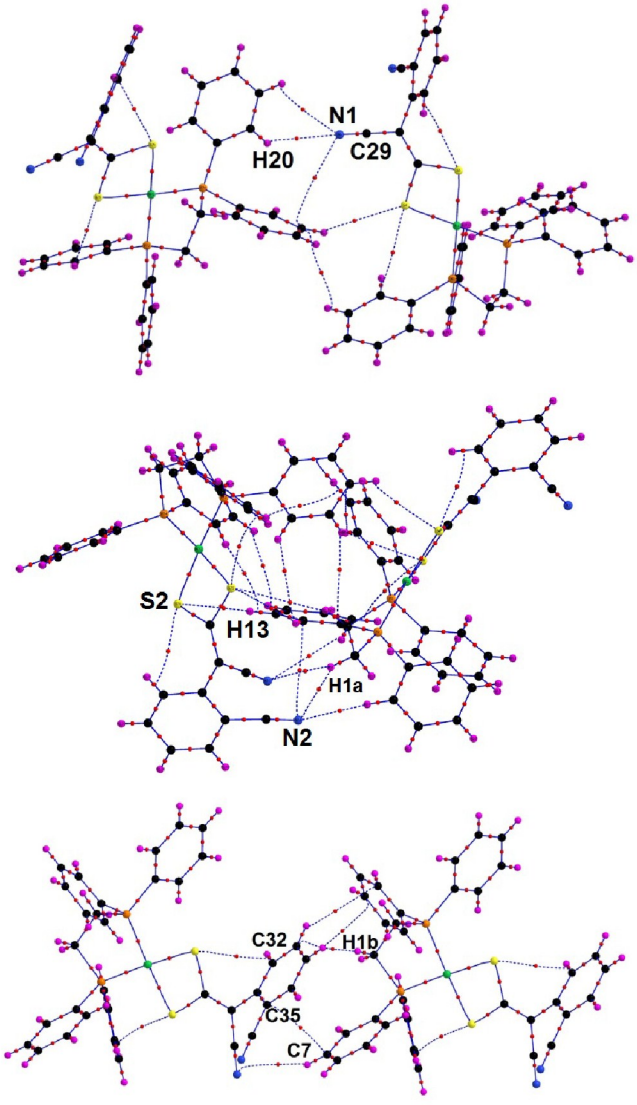

Fig. 6 Molecular graphs for **2** displaying intermolecular (a) C≡N···H (b) C-S···H, C≡N···H and (c) π··· π and C-H··· π interactions.

The analysis of the interaction energies in the crystal structure of **2** by means of dimer units at the BSSE-corrected MP2 level of theory yields an interaction energy of -22 kJ/mol in the C≡N···H dimer (Fig. 3a); the interaction energy of the C-S···H and C≡N···H dimer (Fig. 3b) is calculated to be -66 kJ/mol and the dimer held by π···π and C-H···π (Fig. 3c) is -5 kJ/mol. The high values for the dimer held by C-S···H and C≡N···H (Fig. 3b) indicates an involvement of C-S···H interaction in the system which has high interaction energy. The analysis of the interaction energies in the crystal structure of **3** by means of dimer units at the same level of theory yields an interaction energy for the dimer held by C≡N···H, (py)N···H (Fig. 4) to be -44 kJ/mol and that held by C-S···H and C-H···π interaction (Fig. 4) is -15 kJ/mol. The different intermolecular interaction energies for both the compounds are in the range between 30-15 kJ/mol, which is well beyond the range of H-bond or dipole-dipole interactions.

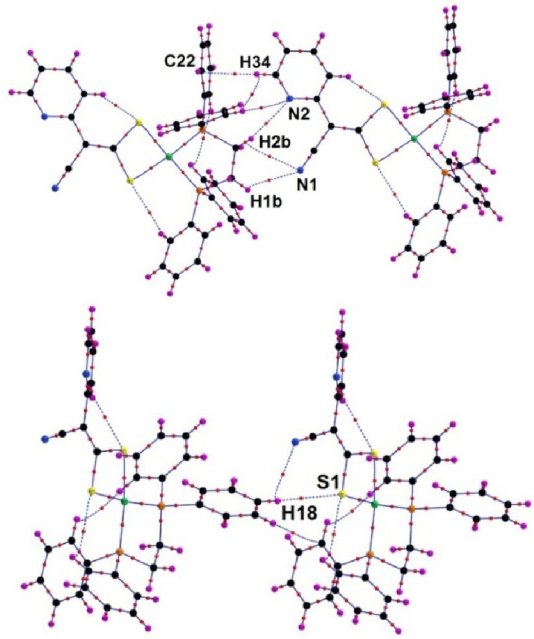

Fig. 7 Molecular graphs for **3** displaying intermolecular (a) C≡N···H; (py)N···H; C-H··· π and (b) C-S···H interactions.

Since the interaction energies obtained by the aforementioned method cannot be estimated independently from each other therefore to evaluate the independent interaction energies and to further confirm the presence of these interactions, bond critical points (bcp) were calculated for dimers (Fig. 6, 7) by using the Atoms in Molecules (AIM) theory.[19] The bond critical points observed between the N and H; S and H; C(π) and C(π) as well as H and C (π) in all the dimers confirms the presence of intermolecular C≡N···H, C-S···H, π···π and C-H···π interaction. The interactions have further been corroborated by calculating the interatomic surfaces between the atoms of interest which bisects at the corresponding bond critical points (Supplementary informations). The values of electron density (ρ); Laplacian ($\nabla^2\rho_{bcp}$); bond ellipticity (ε), Hamiltonian form of the Kinetic Energy (K), Potential Energy density (V), Lagrangian form of Kinetic Energy (G) at the bond critical points between pertinent atoms are presented in Table 1.

From table 1 it is evident that the electron density for all types of interactions at bond critical point (ρ_{bcp}) are less than +0.10 au which indicates a closed shell hydrogen bonding interactions.[20] Additionally, the Laplacian of the electron density $\nabla^2\rho_{bcp}$ in all the cases are greater than zero which indicates the depletion of electron density in the region of contact between the N···H, S···H, C···H and C(π)···C(π) atoms. The bond ellipticity (ε) measures the extent to which the density is preferentially accumulated in a given plane containing the bond path.[20] The ε values for all the interactions indicate that these are not cylindrically symmetrical in nature.[20] The total electron energy density ($H_b = G + V$) associated with these interactions indicates that they are not associated with the significant sharing of electrons and hence confirming the weak non-covalent interaction nature for the two atomic centers.

Table 1. Selected topographical features of inter-molecular C≡N···H, C-S···H, π···π and C-H···π interaction computed at MP2/6-31G**/LANL2DZ level of theory for dimers of **2** and **3**.

Interaction	ρ_{bcp}	$\nabla^2\rho bcp$	(ε)	K	V	G
			2			
C≡N···H	+0.0062	+0.0221	+0.1432	-0.0011	-0.0034	+0.0044
C-S···H	+0.0073	+0.0231	+0.0570	-0.0011	-0.0036	+0.0047
C≡N···H	+0.0085	+0.0291	+0.0575	-0.0012	-0.0049	+0.0035
π···π	+0.0068	+0.0203	+0.7489	-0.0010	-0.0031	+0.0041
CH···π	+0.0066	+0.0221	+0.3064	-0.0012	-0.0030	+0.0043
			3			
(Py)N···H	+0.0080	+0.0251	+0.0445	-0.0009	-0.0044	+0.0054
C≡N···H	+0.0056	+0.0205	+1.2283	-0.0010	-0.0037	+0.0047
CH···π	+0.0082	+0.0251	+0.5430	-0.0011	-0.0040	+0.0051
C-S···H	+0.0050	+0.0183	+0.4082	-0.0010	-0.0030	+0.0043

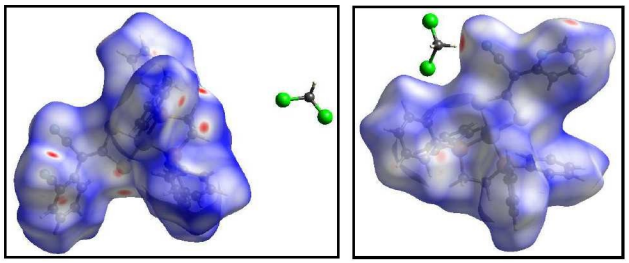

Fig. 8 Hirshfeld surfaces mapped with d_{norm} for **2** (left) and **3** (right).

Hirshfeld Surface Analysis

The Hirshfeld surfaces[17] of **2** and **3** are illustrated in Figure 8, showing surfaces that have been mapped over a d_{norm} range of -0.5 to 1.5 Å. The surfaces are shown as transparent to allow visualization of the aromatic as well as the puckered ring moieties around which they were calculated. The weak interaction information discussed in X-ray crystallography section is summarized effectively in the spots, with the large circular depressions (deep red) visible on the d_{norm} surfaces indicative of hydrogen bonding contacts. The dominant interactions between C-H···π, C–N···H and C–S···H interactions for **2** and **3** can be seen in Hirshfeld surface plots as the red shaded area in Figure 8. The small extent of an area and light colour on the surface indicates weaker and longer contact other than hydrogen bonds.

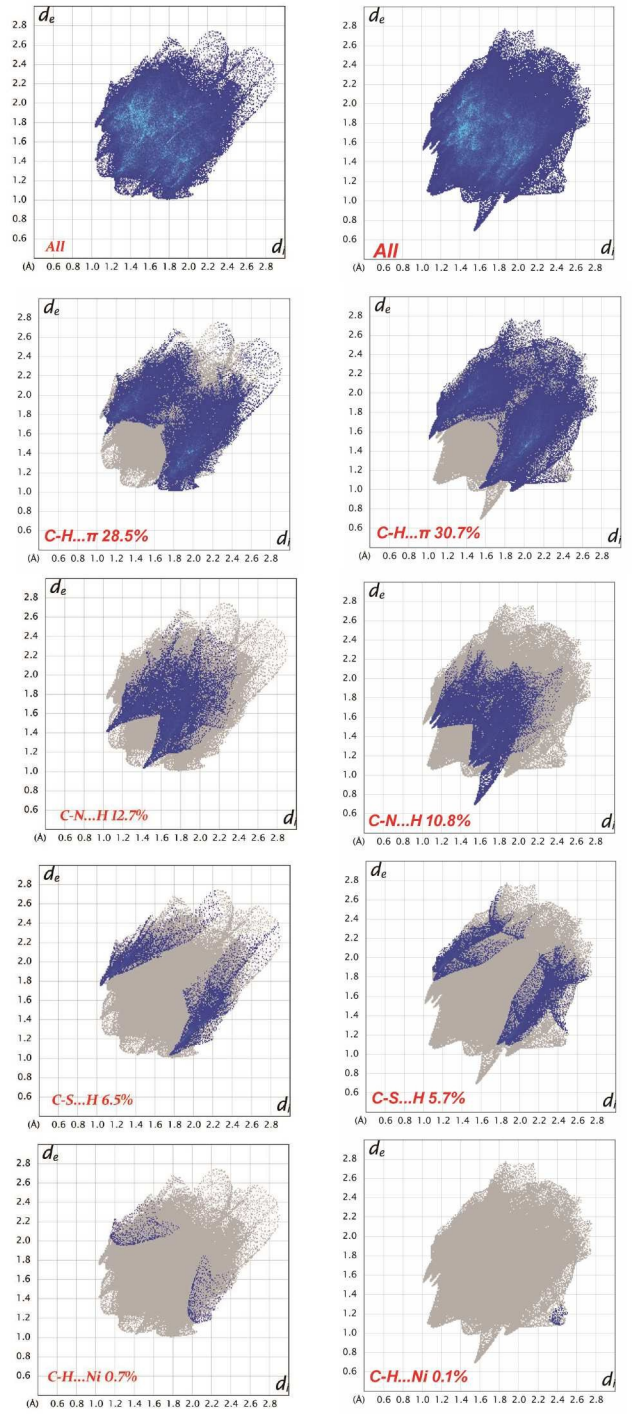

Fig. 9 Fingerprint plots Full, resolved into, C-H···π, C–N···H, C–S···H and C–H···Ni for **2** (left) and **3** (right) showing percentages of contact contributed to the total Hirshfeld surface area of the molecules.

The fingerprint plots[21] for **2** and **3** are presented in Figure 9. The C–N···H and C–S···H intermolecular interactions appear as two distinct spikes of almost equal lengths in the 2D fingerprint

plots in the region 2.03 Å < (d_e + d_i) < 2.47 Å as light sky-blue pattern in full fingerprint 2D plots. Complementary regions are visible in the fingerprint plots where one molecule acts as a donor (d_e> d_i) and the other as an acceptor (d_e< d_i). The fingerprint plots can be decomposed to highlight particular atom pair close contacts. This decomposition enables separation of contributions from different interaction types, which overlap in the full fingerprint. In addition to these interactions a pair of spikes for **2** is observed which corresponds to C−H···Ni anagostic interaction. For **2** the proportions of C−H···π, C−N···H, C−S···H and C−H···Ni interactions comprises of 28.5%, 12.7%, 6.5% and 0.7%, respectively of the total Hirshfeld surface for each molecule. In the case of **3** the proportions of C−H···π, C−N···H, C−S···H and C−H···Ni interactions comprises of 30.7%, 10.8%, 5.7% and 0.1%, respectively of the total Hirshfeld surface for each molecule. The C-H···Ni anagostic interaction is not evident at the QTAIM level. However, the Hirshfeld surface analysis indicates presence of anagostic interaction but small. Therefore, we sought additional, independent evidence from orbital structure analysis.

To gain further additional insight into the C−H···Ni anagostic interaction into the compounds **2** and **3** the Wieberg bond indices and Mayer bond orders for the both the *ortho* C–H bonds of the aromatic rings of dppe ligand undergoing and not displaying any anagostic interaction were calculated (Fig. 5). The pertinent results of the calculations are presented in table 2.

Table 2. The calculated Wieberg bond indices and Mayer Bond Orders between the atoms of interest for **2** and **3**.

Bonding	Bond Length (Calc.)	Wieberg Bond Indices	Mayer Bond Order	Natural Charges	
		2			
C4–H4	**1.0872**	**0.9171**	**0.9323**	**C4**	**-0.1730**
C8–H8	1.0862	0.9293	0.9474	H8	0.2048
C26–H26	**1.0875**	**0.9185**	**0.9406**	**C26**	**-0.1583**
C22–H22	1.0860	0.9298	0.9470	H22	0.2077
Ni···H4	**2.9473**	**0.0043**	**0.0079**	**H4**	**0.2203**
Ni···H26	**2.9169**	**0.0047**	**0.0086**	**H26**	**0.2216**
		3			
C20–H20	**1.0874**	**0.9153**	**0.9364**	**C20**	**-0.1556**
C16–H16	1.0868	0.9312	0.9463	H16	0.2040
C14–H14	**1.0876**	**0.9188**	**0.9392**	**C14**	**-0.1730**
C10–H10	1.0872	0.9268	0.9441	H10	0.2102
Ni···H20	**2.8296**	**0.0044**	**0.0057**	**H20**	**0.2287**
Ni···H14	**2.7637**	**0.0060**	**0.0119**	**H14**	**0.2203**

The C-H bond parameters in bold are involved in anagostic interactions.

From table 2 it is evident the C-H bonds involved in anagostic interactions (shown in bold) have relatively longer bond lengths than those C-H bonds which are not involved in the anagostic interactions. Although these bond length differences are showing very small deviations but they are noticeable. The Wieberg bond indices and Mayer bond order for the C-H bonds showing anagostic interactions are relatively smaller than C-H bonds not showing this interaction. These computational parameters give evidences for the involvement of the *ortho*-C–H bonds of one side to undergo anagostic interactions. Also the Ni···H Wieberg bond indices and Mayer bond order for **3** is relatively larger than **2** which indicates that the strength of anagostic interaction in **3** is relatively greater than **2**.

Since the anagostic interactions are predominantly electrostatic in nature which leads to downfield shift in δ_H of the C-H bond[18], therefore the natural charges on the both the coordinated and uncoordinated *ortho*-hydrogen atoms was computed (table 2). The calculations indicate the relative depletion of electron density on the *ortho*-hydrogen atoms undergoing the anagostic interactions in comparison to the *ortho*-hydrogen lying far apart from the Ni center. This further corroborates the existence of anagostic interactions in both **2** and **3**.

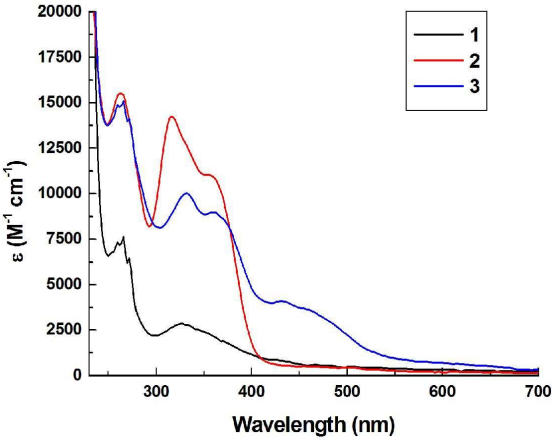

Fig. 10 Electronic absorption spectra of compounds **1-3** recorded in 10^{-4} M dichloromethane solution.

Electronic spectra and photoluminescent properties

The electronic absorption spectra for all of the three compounds recorded in dichloromethane are shown in Fig. 10. In all the spectra, the bands observed from 230-400 nm are attributed to intraligand charge transfer transition.[14, 22, 23] The weak broad absorptions at near 400 nm is due to ligand-to-metal charge transfer (LMCT) and are consistent with square planar geometry about the metal center.[24] The additional broad band at ~ 450 nm in **3** might be due the presence of pyridyl ring in the dithiolate ligand.

Upon excitation at 320 nm, a broad emissions at 370 nm, 415 nm and 400 nm observed for compounds **1, 2** and **3** respectively, were observed which is in persistent of earlier reports (Fig. 11a).[14,22] The photoluminescence spectra for all the compounds were also recorded in solid state (Fig. 11). When excited at 320 nm, all the three compounds exhibited emissions at ~501, 509 and 518 nm, respectively (Fig. 11b). From the photoluminescence spectra recorded in solid state it is clearly evident that in comparison to the solution phase the emissions in solid state are relatively red shifted. The red-shift may in the solid state emissions may be due to the involvement of non-covalent interactions operating in the solid state.

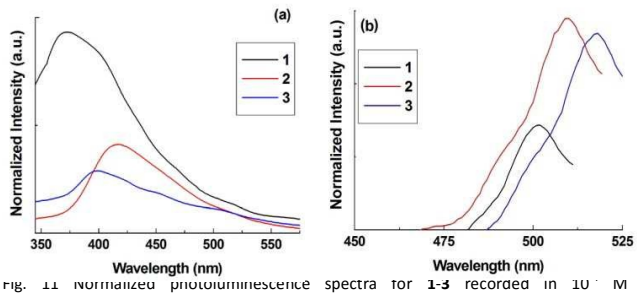

Fig. 11 Normalized photoluminescence spectra for **1-3** recorded in 10^{-5} M dichloromethane solution **(a)**; in solid state **(b)**.

Conclusion

The crystallographic studies of the reported compounds demonstrated various supramolecular structural diversities as a function of the substitution present on the dithiolate ligands. Incorporation of pyridyl ring in the molecular framework of **3** leads to the chain motifs bonded by both C≡N···H, (py)N···H interactions. Attempts were made to address the nature of weak inter- and intra-molecular interactions in the newly synthesized compounds using Hirshfeld surface analyses alongwith the DFT and AIM theory calculations. The fingerprint plots also allows a more detailed scrutiny by displaying all the intermolecular interactions within the crystal and therefore are suitable for analyzing the changes in crystal packing in the molecular systems, under investigation. The anagostic interactions observed in the X-ray structures were proved using the fingerprint plots, Wieberg bond indices and Mayer bond order calculations. Based on our findings it can be concluded that by careful engineering the nature of ring and incorporation of the appropriate functionalities on these aromatic rings, the architecture of the self-assembled hydrogen bonded and π···π stacking interactions can be tuned. These interactions in solid state may lead to red shift in the photoluminescence emissions in comparison to the solution phase photoluminescence.

Experimental

Materials and methods

All chemical reagents are commercially available and were used without further purification. Elemental analyses were performed on a Perkin-Elmer 240 C, H, N analyzer. Infrared spectra were recorded as KBr pellets on a Varian 3100 FTIR. ^{1}H, ^{13}C and ^{31}P NMR spectra were recorded on JEOL AL300 FTNMR spectrophotometers. Chemical shifts were reported in parts per million using TMS as internal standard for ^{1}H and ^{13}C NMR and phosphoric acid for ^{31}P NMR. The electronic absorption and photoluminescent spectra in dichloromethane solution were recorded using a SPECORD 210 PLUS BU and CARY Eclipse spectrophotometers, respectively.

Syntheses

[Ni(dppe)(benzylcyanidedithiolate)] (1)

To a solution of benzyl cyanide (0.621 g, 0.53 mmol) in THF (10 mL), DBU (0.16 mL, 1.06 mmol) was added under nitrogen atmosphere. The solution was stirred at room temperature for 5 min followed by the addition of CS_2 (0.04 mL, 0.53 mmol). The solution, which turned yellow, was stirred for an additional 2 h, after which it was transferred dropwise through dropping funnel to a solution of [Ni(dppe)Cl_2] (0.280 g, 0.53 mmol) in dichloromethane (50 mL). The resulting solution turned red. The solution was stirred at room temperature for 1 day, after which solvent was removed using a rotary evaporator and redissolved in 5 mL dichloromethane and filtered through celite and eventually precipitated by the addition of 25 mL petroleum ether.

1 Dark red solid (0.282 g, 82% yield); m. p. 198 °C; IR (KBr, cm^{-1}): 2198 (-C≡N), 1437 (C=CS_2), 1107 (CS_2). ^{1}H NMR (300 MHz, $CDCl_3$): δ = 7.74 (m, 5H, C_6H_5) 7.27-7.08 (m, 20H, C_6H_5), 2.69 (s, 4H, -CH_2-CH_2-). ^{13}C NMR (75.45 MHz, $CDCl_3$) δ = 199.8 (CS_2), 151.3, 151.2, 151.0, 150.4 (-C_6H_5), 138.2, 132.4, 129.5 (P-C_6H_5), 121.5 (-C≡N), 121.3 (C=C), 25.6 (-CH_2-CH_2-). ^{31}P{^{1}H} NMR (121.50 MHz, $CDCl_3$): δ = 58.46. Elemental analysis for $C_{35}H_{29}NNiP_2S_2.0.5CH_2Cl_2$ (M_r = 697.05): calcd: C, 61.87%; H, 4.62%; N, 2.00 %; S, 9.18%. Found: C, 62.33%; H, 4.72%; N, 2.57%; S, 9.89%.

[Ni(dppe)(2-cyanobenzylcyanidedithiolate)] (2)

The similar procedure mentioned for the synthesis of **1** was adopted for the synthesis of **2** except that 2-cyanobenzyl cyanide (0.753 g, 0.53 mmol) was used instead of benzyl cyanide.

2 Orange red solid (0.307 g, 88% yield); m. p. 206 °C; IR (KBr, cm^{-1}): 2200, 2090 (-C≡N), 1430 (C=CS_2), 1099 (CS_2). ^{1}H NMR (300 MHz, $CDCl_3$): δ = 9.12 (s, 1H, C_6H_4), 8.71-8.68 (t, 1H, C_6H_4), 8.34 (s, 1H, C_6H_4), 8.21 (s, 1H, C_6H_4),7.30-7.28 (m, 20H, C_6H_5), 2.64 (s, 4H, -CH_2-CH_2-).^{13}C NMR (75.45 MHz, $CDCl_3$) δ= 201.2 (CS_2), 152.1, 151.6, 151.0, 150.2, (-C_6H_4), 138.2, 132.4, 129.5 (P-C_6H_5), 123.8 (C=C), 119.0 (-C≡N), 117.0 (-C≡N), 25.4 (-CH_2-CH_2-). ^{31}P{^{1}H} NMR (121.50 MHz, $CDCl_3$): δ = 57.92. Elemental analysis for $C_{36}H_{28}N_2NiP_2S_2.0.6CH_2Cl_2$ (M_r = 724.35): calcd: 60.69%; H, 4.06%; N, 3.87%; S, 8.85%. Found: 61.48%; H, 4.57%; N, 4.12%; S, 9.76%.

[Ni(dppe)(pyridine-2-cyanidedithiolate)] (3)

The similar procedure mentioned for the synthesis of **1** was adopted for the synthesis of **3** except that pyridine-2-acetonitrile (0.626 g, 0.53 mmol) was used instead of benzyl cyanide.

3 dark red brown solid (0.286 g, 83% yield); m. p. 202 °C; IR (KBr, cm^{-1}): 2191 (-C≡N), 1438 (C=CS_2), 1102 (CS_2). ^{1}H NMR (300 MHz, $CDCl_3$) δ =8.57 (s,1H, py), 7.72 (s,1H, py), 7.41 (s, 1H, py), 7.26 (s, 1H, py), 7.30-7.28 (m, 20H, C_6H_5), 2.64 (s, 4H, -CH_2-CH_2-).^{13}C NMR (75.45 MHz, $CDCl_3$) δ= 198.0 (CS_2), 150.6, 149.9, 137.4, 123.0, 122.3 (-C_6H_4), 138.2, 132.4, 129.5 (P-C_6H_5), 122.8 (C=C), 117.2 (-C≡N), 25.4 (-CH_2-CH_2-). ^{31}P{^{1}H} NMR (121.50 MHz, $CDCl_3$): δ = 56.53. Elemental analysis for $C_{34}H_{29}N_2NiP_2S_2.0.25CH_2Cl_2$ (M_r = 671.61): calcd: C, 61.25%; H, 4.43%; N, 4.17%; S, 9.55%. Found C, 62.45%; H, 4.72%; N, 4.98%; S, 10.82%.

X-ray Crystallography

Intensity data for **2** and **3** were collected at 150(2) K on an Nonius Kappa CCD single crystal diffractometer using graphite monochromated Mo-Kα radiation λ = 0.71073 Å. Unit cell determination, data collection and data reduction were performed using the Nonius software.[25] For both structures a symmetry-related (multi-scan) absorption correction had been applied. The structures were solved by direct methods (SIR97)[26] and refined by a full-matrix least-squares procedure based on F^2 (Shelxl-2014).[27] All non-hydrogen atoms were refined anisotropically. Hydrogen atoms were placed onto calculated positions and refined using a riding model. Additional programmes used for analysing data and graphically manipulating them included: SHELXle[28] and ORTEP 3 for windows.[29] The compound **3** was refined as a 2-component inversion twin in the ratio 1:2. The compound co-crystallises with 0.35 CH_2Cl_2 which is disordered over two sites with occupation factor of 25% for part 1 and 10% for part 2. Atom Cl2 is shared by both parts and C42 of the solvent molecule (from part 2) was refined with ADP restraints.

Crystal Data **2**: $C_{36}H_{28}N_2NiP_2S_2.0.6CH_2Cl_2$, M = 724.33, Monoclinic, $P2_1/n$, a = 12.0561(2) Å, b = 13.4846(3) Å, c = 21.0459(5) Å, β = 97.4474(9)°, V = 3392.60(12) Å^3, Z=4, D_{calc}=1.418 mg m^{-3}, F(000) = 1493, crystal size 0.230 × 0.180 × 0.150 mm, reflections collected 34875, independent reflections 5981 [$R_{(int)}$ = 0.1169], Final indices [I> 2σ(I)] R_1 = 0.0505 wR_2 = 0.1151, R indices (all data) R_1 = 0.0922, wR_2 = 0.1331, gof 1.032, Largest difference peak and hole 0.672 and -0.568 e Å^{-3}. **CCDC No. 1403943**

Crystal Data **3**: $C_{34}H_{29}N_2NiP_2S_2.0.35CH_2Cl_2$, M = 679.08, Orthorhombic, F2dd, a = 11.7944(1) Å, b = 18.1645(2) Å, c = 61.6538(8) Å, V = 13208.7(3) Å^3, Z=4, D_{calc}=1.366 mg m^{-3}, F(000) = 5611, crystal size 0.600 × 0.500 × 0.300 mm, reflections collected 32060, independent reflections 7432 [$R_{(int)}$ = 0.0638], Final indices [I> 2σ(I)] R_1 = 0.0346 wR_2 = 0.0707, R indices (all data) R_1 = 0.0481, wR_2 = 0.0758, gof 1.073, Largest difference peak and hole 0.343 and -0.309 e Å^{-3}. **CCDC No. 1403944**

Computational details

Molecular geometries were optimized at the level of density functional theory (DFT) using the B3LYP functional.[30] The split valence basis sets, 6-31G** were used at all C, N, S, P and H atom centers. LANL2DZ basis set was used for the Ni atom. The intermolecular interaction energies have been estimated at the MP2 level of theory.[31] For the interaction energy calculations, the interaction distances have been fixed for the dimer while all other degrees of freedom were relaxed in the geometry optimization. The stabilization energies (ΔE_{dimer} and ΔE_{trimer}) for dimeric and trimeric motifs involving the 2 and 3 molecules, respectively were calculated using the formula $\Delta E_{dimer} = E_{dimer} - (2 \times E_{monomer})$ where $E_{monomer}$, E_{dimer} are the energies of the monomer and dimer motifs. $E_{monomer}$ was calculated by optimizing a single molecule at the same level of theory. The intermolecular interaction strengths are significantly weaker than either ionic or covalent bonding, therefore it was essential to do basis set superposition error (BSSE) corrections. The BSSE corrections in the interaction energies were done using Boys-Bernardi scheme. In this paper all the interaction energies have been reported after BSSE correction.[32] All computational experiments have been performed using the Gaussian 09 programme.[33]

Hirshfeld Surface Analysis

Molecular Hirshfeld surfaces[34] in the crystal structure were constructed on the basis of the electron distribution calculated as the sum of spherical atom electron densities.[35,36] For a given crystal structure and a set of spherical atomic densities, the Hirshfeld surface is unique.[37] The normalized contact distance (d_{norm}) based on both d_e and d_i (where d_e is distance from a point on the surface to the nearest nucleus outside the surface and d_i is distance from a point on the surface to the nearest nucleus inside the surface) and the vdW radii of the atom, as given by eq 1 enables identification of the regions of particular importance to intermolecular interactions.[34] The combination of d_e and d_i in the form of two-dimensional (2D) fingerprint plot[38,39] provides a summary of intermolecular contacts in the crystal.[34] The Hirshfeld surfaces mapped with d_{norm} and 2D fingerprint plots were generated using the Crystal-Explorer 3.1.[40] Graphical plots of the molecular Hirshfeld surfaces mapped with d_{norm} used a red-white-blue colour scheme, where red highlight shorter contacts, white represents the contact around vdW separation, and blue is for longer contact.[41]

$$d_{norm} = \frac{d_i - r_i^{vdW}}{r_i^{vdW}} + \frac{d_e - r_e^{vdW}}{r_e^{vdW}} \quad (1)$$

Acknowledgements

AK is grateful to Department of Science and Technology, New Delhi for the financial support through project no. SB/FT/CS-018/2012.

Notes and references

‡Footnotes relating to the main text should appear here. These might include comments relevant to but not central to the matter under discussion, limited experimental and spectral data, and crystallographic data.

1 (a) D. Coucouvanis, *Prog. Inorg. Chem.*, 1970, **11**, 233; 1979, 26, 301; (b) G. Hogarth, *Prog. Inorg. Chem.*, 2005, **53**, 71.

2 (a) J. Cookson and P. D. Beer, *Dalton Trans.*, 2007, **15**, 1459; (b) E. R. T. Tiekink and I. Haiduc, *Prog. Inorg. Chem*., 2005, **54**, 127; (b) C. S. Lai and E. R. T. Tiekink, CrystEngComm, 2003, **5**, 253; (c) E. R. T. Tiekink and I. Haiduc, Prog. Inorg. Chem., 2005,**54**, 127; (d) C. S. Lai and E. R. T. Tiekink, CrystEngComm, 2003, **5**, 253; (e) T. Okubo, N. Tanaka, K. H. Kim, H. Yone, M. Maekawa and T. Kuroda-Sowa, *Inorg. Chem.*, 2010, **49**, 3700; (f) T. Okubo, H. Anma, N. Tanaka, K. Himoto, S. Seki, A. Saeki, M. Maekawa and T. Kuroda-Sowa, *Chem. Commun.*, 2013, **49**, 4316; (g) P. I. Clemenson, *Coord. Chem. Rev.*, 1990, **106**, 171.

3 (a) R. Kato, *Chem. Rev.*, 2004, **104** , 5319–5346; (b) M. Bousseau, L. Valade, J. P. Legros, P. Cassoux, M. Garbauskas and L. V. Interrante, *J. Am. Chem. Soc.*, 1986, **108**, 1908–1916; (c) K. Kubo, T. Shiga, T. Yamamoto, A. Tajima, T.

Moriwaki, Y. Ikemoto, M. Yamashita, E. Sessini, M. L. Mercuri, P. Deplano, Y. Nakazawa and R. Kato, *Inorg. Chem.*, 2011, **50**, 9337–9344; (d) M. Saeki, K. Dai, S. Ichimura, Y. Tamaki, K. Tomonob and K. Miyamura, *Dalton Trans.*, 2014, **43**, 17067-17074.

4 (a) M. Shatruk and L. Ray, *Dalton Trans.*, 2010, **39**, 11105-11121.

5 (a) J. Zhang, P. Du, J. Schneider, P. Jarosz and R. Eisenberg, *J. Am. Chem. Soc.*, 2007, **129 (25),** 7726–7727; (b) J. A. Weinstein, M. T. Tierney,E. S. Davies, K. Base, A. A. Robeiro and M. W. Grinstaff, *Inorg. Chem.*, 2006, **45**, 4544–4555; (c) Y-D. Chen, L-Y. Zhang, L-X. Shi and Z-N. Chen, *Inorg. Chem.*, 2004, **43**, 7493–7501; (d) Y-D. Chen, Y-H. Qin, L-Y Zhang, L-X. Shi and Z-N. Chen, *Inorg. Chem.*, 2004, **43**, 1197–1205; (e) J. Vicente, M. T. Chicote, and S. Huertas, *Inorg. Chem.*, 2001, **40**, 6193–6200; (f) K-S. Shin, K-I. Son, J. I. Kim, C. S. Hong, M. Suh and D-Y. Noh, *Dalton Trans.*, 2009, 1767-1775; (g) V. F. Plyusnin, I. P. Pozdnyakov, V. P. Grivin, A. I. Solovyev, H. Lemmetyinen, N. V. Tkachenko and S. V. Larionovd, *Dalton Trans.*, 2014, **43**, 17766-17774.

6 (a) M. Akhtar, J. Akhter, M. A. Malik, P. O'Brien, F. Tuna, J.Raftery and M. Helliwell, *J. Mater. Chem.*, 2011, **21**, 9737-9745; (b) M. Akhtar, M. A. Malik, F. Tuna and P. O'Brien, *J. Mater. Chem. A*, 2013, **1**, 8766-8774; (c) S. Saeed, N. Rashid, R. Hussain, M. A. Malik, P. O'Brien and W-T. Wong, *New J. Chem.*, 2013, **37**, 3214-3221; (d) C. G. Morales-Guio and X. Hu, *Acc. Chem. Res.*, 2014, **47 (8)**, 2671–2681; (e) J. P. Shupp, A. S. Kinne, H. D. Arman and Z. J. Tonzetich, *Organometallics*, 2014, **33 (19),** 5238–5245; (f) R. Lv, J. A. Robinson, R. E. Schaak, D. Sun, Y. Sun, T. E. Mallouk, and M. Terrones, *Acc. Chem. Res.*, 2015, **48 (1)**, 56–64; (g) N. P. Dasgupta, X. Meng, J. W. Elam and A. B. F. Martinson, *Acc. Chem. Res.*, 2015, **48 (2)**, 341–348.

7 (a) K. Ramasamy, M. A. Malik, N. Revaprasadu and P. O'Brien *Chem. Mater.*, 2013, **25 (18)**, 3551–3569; (b) K. Ramasamy, M. A. Malik and P. O'Brien, *Chem. Commun.*, 2012, **48**, 5703-5714.

8 A. Henckens, K. Colladet, S. Fourier, T. J. Cleij, L. Lutsen, J. Gelan and D. Vanderzande, *Macromolecules*, 2005, **38**, 19.

9 (a) G. R. Desiraju, *Chem. Commun.*, 2005, 2995; (b) C. R. Kaiser, K. C. Pais, M. V. N. de Souza, J. L. Wardell, S. M. S. V. Wardell and E. R. T. Tiekink, *CrystEngComm*, 2009, **11**, 1133; (c) Y. R. Zhong, M. L. Cao, H. J. Mo and B. H. Ye, *Cryst. Growth Des.*, 2008, **8**, 2282; (d) S. Takahashi, T. Jukurogi, T. Katagiri and K. Uneyama, *CrystEngComm*, 2006, **8**, 320; (e) A. N. Sokolov, T. Friscic, S. Blais, J. A. Ripmeester and L. R. MacGillivray, *Cryst. Growth Des.*, 2006, **6**, 2427; (f) J. W. Steed and J. L. Atwood, *Supramolecular Chemistry*, VCH, New York, 2000; (g) D. R. Armstrong, M. G. Davidson and D. Moncrief, *Angew. Chem., Int. Ed. Engl.*, 1995, **34**, 478.

10 (a) E. R. T. Tiekink and J.-Z. Schpector, *Chem. Commun.*, 2011, **47**, 6623; (b) M. Mitra, P. Manna, A. Das, S. K. Seth, M. Helliwell, A. Bauzá, S. R. Choudhury, A. Frontera and S. Mukhopadhyay, *J. Phys. Chem. A*, 2013, **117**, 5802–5811; (c) M. Mitra, P. Manna, A. Bauzá, P. Ballester, S. K. Seth, S. R. Choudhury, A. Frontera and S. Mukhopadhyay, *J. Phys. Chem. B*, 2014, **118**, 14713–14726; (d) P. Manna, S. K. Seth, A. Bauzá, M. Mitra, S. R. Choudhury, A. Frontera and S. Mukhopadhyay, *Cryst. Growth Des.*, 2014, **14**, 747–755; (e) P. Manna, S. K. Seth, M. Mitra, S. R. Choudhury, A. Bauzá, A. Frontera and S. Mukhopadhyay, *Cryst Growth Des.*, 2014, **14**, 5812–5821.

11 (a) H. V. Huynh, L. R. Wong and P. S. Ng, *Organometallics*, 2008, **27**, 2231; (b) W. Yao, O. Eisenstein and R. H. Crabtree, *Inorg. Chim. Acta*, 1997, **254**, 105; (d) J. Saßmannshausen, *Dalton Trans.*, 2012, **41**, 1919; (e) Y. Zhang, J. C. Lewis, R. G. Bergman, J. A. Ellman and E. Oldfield, *Organometallics*, 2006, **25**, 3515; (f) K. A. Siddiqui and E. R. T. Tiekink, *Chem. Commun.*, 2013, **49**, 8501; (g) S. Schöler, M. H. Wahl, N. I. C. Wurster, A. Puls, C. Hättig and G. Dyker, *Chem. Commun.*, 2014, **50**, 5909; (h) M. G. D. Holaday, G. Tarafdar, A. Kumar, M. L. P. Reddy and A. Srinivasan, *Dalton Trans.*, 2014, **43**, 7699; (i) S. K. Seth, I. Saha, C. Estarellas, A. Frontera, T. Kar, and S. Mukhopadhyay, *Cryst. Growth Des.*, 2011, **11**, 3250–3265; (j) P. Manna, S. K. Seth, A. Das, J. Hemming, R. Prendergast, M. Helliwell, S. R. Choudhury, A. Frontera, and S. Mukhopadhyay, *Inorg. Chem.*, 2012, **51**, 3557−3571; (k) M. Mitra, P. Manna, S. K. Seth, A. Das, J. Meredith, M. Helliwell, A. Bauzá, S. R. Choudhury, A. Frontera and S. Mukhopadhyay, *CrystEngComm*, 2013, **15**, 686-696; (l) S. K. Seth, *CrystEngComm*, 2013, **15**, 1772-1781; (m) S. K. Seth , D. Sarkar and T. Kar, *CrystEngComm*, 2011, **13**, 4528-4535; (n) P. Manna, S. K. Seth, M. Mitra, A. Das, N. J. Singh, S. Ray Choudhury, T. Kar and S. Mukhopadhyay, *CrystEngComm*, 2013, **15**, 7879-7886; (o) S. K. Seth , P. Manna , N. J. Singh , M. Mitra , A. D. Jana , A. Das , S. R. Choudhury , T. Kar , S. Mukhopadhyay and K. S. Kim, *CrystEngComm*, 2013, **15**, 1285-1288; (p) S. K. Seth , D. Sarkar , A. Roy and T. Kar, *CrystEngComm*, 2011, **13**, 6728-6741; (q) S. K. Seth, *J. Mol. Str.*, 2014, 1070, 65-74.

12 J. D. E.T.Wilton-Ely, D. Solanki, E. R. Knight, K. B. Holt, A. L. Thompson and G. Hogarth, *Inorg. Chem.*, 2008, **47**, 9642-9653.

13 E. R. Knight, E. R. Leung, Y. H. Lin, A. R. Cowley, D. J. Watkin, A. L. Thompson, G. Hogarth and J. D. E. T. Wilton-Ely, *Dalton Trans.*, 2009, 3688-3697.

14 R. Chauhan, M. Trivedi, J. Singh, K. C. Molloy, G. Kociok-Köhn, U. P. Mulik, D. P. Amalnerkar and A. Kumar, *Inorg. Chim. Acta*, 2014, **415**, 69-74.

15 S. Huertas, M. Hissler, J. E. McGarrah, R. J. Lachicotte and R. Eisenberg, *Inorg. Chem.*, 2001, **40**, 1183-1188.

16 (a) M. Trivedi, G. Singh, A. Kumar, N. P. Rath, *Dalton Trans.*, 2014, **43**, 13620-13629; (b) M. Trivedi, G. Singh, A. Kumar, N. P. Rath, *Dalton Trans.*, 2013, **42**, 12849-112852.

17 (a) S. K. Seth, D. Sarkar, A. D. Jana and T. Kar, *Cryst. Growth Des.*, 2011, **11**, 4837–4849; (b) M. Mitra, S. K. Seth, S. R. Choudhury, P. Manna, A. Das, M. Helliwell, A. Bauzá, A. Frontera and S. Mukhopadhyay, *Eur. J. Inorg. Chem.*, 2013, 4679–4685; (c) S. K. Seth, *Inorg. Chem. Commun.*, 2014, **43**, 60–63.

18 (a) M. Brookhart, M. L. H. Green and G. Parkin, *Proc. Natl. Acad. Sci. U. S. A.*, 2007, **104**, 6908-6914; (b) H. V. Huynh, L. R. Wong and P. S. Ng, *Organometallics*, 2008, **27**, 2231; (c) W. I. Sundquist, D. P. Bancroft and S. J. Lippard, *J. Am. Chem. Soc.*, 1990, 112, 1590-1596; (d) D. Braga, F. Grepioni, E. Tedesco, K. Biradha and G. R. Desiraju, *Oganometallics*, 1997, 16, 1846-1856.

19 R. F. W. Bader, *Atoms in Molecules: A Quantum Theory*; Oxford University Press: New York, 1990.

20 C. F. Matta and R. J. Boyd, *The Quantum Theory of Atoms in Molecules*: From Solid State to DNA and Drug Design; Wiley VCH, VerlagGmbh& Co. KGaA: Germany, 2007.

21 (a) S. K. Seth, *J. Sol. State Chem.*, 2014, **220**, 149–156; (b) T. Samanta, L. Dey, J. Dinda, S. K. Chattopadhyay, S. K. Seth, *J. Mol. Struc.*, 2014, **1068**, 58–70; (c) S. K. Seth, *J. Mol. Struc.*, 2014, **1064**, 70–75.

22 S. P. Kaiwar, A. Vodacek, N. V. Blough and R. S. Pilato, *J. Am. Chem. Soc.*, 1997, **119**, 3311–3316.

23 E. G. Bakalbassis, G. A. Katsoulos and C. A. Tsipis, *Inorg. Chem.*, 1987, **26**, 3151–3158.

24 R. S. Amim, M. R. L. Oliveira, G. J. Perpetuo, J. Janczak, L. D. L. Miranda and M. M. M. Rubinger, *Polyhedron*, 2008, **27**, 1891–1897.

25 DENZO-SCALEPACK Z. Otwinowski and W. Minor, "Processing of X-ray Diffraction Data Collected in Oscillation Mode", Methods in Enzymology, Volume 276: Macromolecular

Crystallography, part A, p.307-326, 1997, C.W. Carter, Jr. & R. M. Sweet, Eds., Academic Press.
26 SIR97 - A. Altomare,M. C. Burla, M. Camalli,G. L. Cascarano, C.Giacovazzo, A.Guagliardi, A. G. G.Moliterni,G. Polidori and R. Spagna, *J. Appl. Crystallogr.*, 1999, **32**, 115-119.
27 G. M. Sheldrick, *ActaCryst*, 2015, **C71**, 3-8.
28 C. B. Hübschle, G. M. Sheldrick and B. Dittrich ShelXle: a Qt graphical user interface for SHELXL *J. Appl. Cryst.*, 2011, **44**, 1281-1284.
29 ORTEP3 for Windows L. J. Farrugia, *J. Appl. Crystallogr.*, 1997, **30**, 565.
30 (a) A. D. Becke, *J. Chem. Phys.*, 1993, **98**, 5648; (b) C. T. Lee, W. T. Yang and R. G. Parr, *Phys. Rev. B: Condens. Matter Mater. Phys.*, 1998, **37**, 1133.
31 M. Head-Gordon, J. A. Pople and M. J. Frisch, *Chem. Phys. Lett.*, 1988, **153**, 503-506.
32 S. F. Boys and F. Bernardi, *Mol. Phys.,* 1970, **19**, 553.
33 M. J. Frisch, G. W. Trucks, H. B. Schlegel, G. E. Scuseria, M. A. Robb, J. R. Cheeseman, J. A. Montgomery, T. Vreven Jr., K. N. Kudin, J. C. Burant, J. M. Millam, S. S. Iyengar, J. Tomasi, V. Barone, B. Mennucci, M. Cossi, G. Scalmani, N. Rega, G. A. Petersson, H. Nakatsuji, M. Hada, M. Ehara, K. Toyota, R. Fukuda, J. Hasegawa, M. Ishida, T. Nakajima, Y. Honda, O. Kitao, H. Nakai, M.; Klene, X. Li, J. E. Knox, H. P. Hratchian, J. B. Cross, V. Bakken, C. Adamo, J. Jaramillo, R. Gomperts, R. E. Stratmann, O. Yazyev, A. J. Austin, R. Cammi, C. Pomelli, J. W. Ochterski, P. Y. Ayala, K. Morokuma, G. A. Voth, P. Salvador, J. J. Dannenberg, V. G. Zakrzewski, S. Dapprich, A. D. Daniels, M. C. Strain, O. Farkas, D. K. Malick, A. D. Rabuck, K. Raghavachari, J. B. Foresman, J. V. Ortiz, Q. Cui, A. G. Baboul, S. Clifford, J. Cioslowski, B. B. Stefanov, G. Liu, A. Liashenko, P. Piskorz, I. Komaromi, R. L. Martin, D. J. Fox, T. Keith, M. A. Al-Laham, C. Y. Peng, A. Nanayakkara, M. Challacombe, P. M. W. Gill, B. Johnson, W. Chen, W. M. Wong, C. Gonzalez and J. A. Pople, Gaussian, Inc., Wallingford CT, 2004.
34 M. A. Spackman and J. J. McKinnon, *CrystEngComm*, 2002, **4**, 378-392.
35 M. A. Spackman and P. G. Byrom, *Chem. Phy. Lett.*, 1997, **267**, 309.
36 J. J. McKinnon, A. S. Mitchell, and M. A. Spackman, *Chem-Eur. J.*, 1998, **4**, 2136-2141.
37 J. J. McKinnon, M. A. Spackman and A. S. Mitchell, *Acta Crystallogr. Sec. B*, 2004, **60**, 627-668.
38 A. L. Rohl, M. Moret, W. Kaminsky, K. Claborn, J. J. McKinnon and B. Kahr, *Cryst. Growth Des.*, 2008, **8**, 4517-4525.
39 A. Parkin, G. Barr, W. Dong, C. J. Gilmore, D. Jayatilaka, J. J. McKinnon, M. A. Spackman and C. C. Wilson, *CrystEngComm*, 2007, **9**, 648-652.
40 S. K. Wolff, D. J. Greenwood, J. J. McKinnon, D. Jayatilaka and M. A. Spackman, *Crystal Explorer 3.1*; University of Western Australia: Perth, Australia, **2012**.
41 J. J. Koenderink and A. J. van Doorn, *Image Vision Comput.* 1992, ***10***, 557-564.